J|A|C|S ARTICLES

Published on Web 12/17/2009

Helical Structure of Xylose-DNA

Amutha Ramaswamy,[†,§] Mathy Froeyen,[‡] Piet Herdewijn,[‡] and Arnout Ceulemans*[,†]

INPAC institute for Nanoscale Physics and Chemistry and Quantum Chemistry Group of K. U. Leuven, Celestijnenlaan 200F, B-3001 Leuven, Belgium, Laboratory for Medicinal Chemistry, K. U. Leuven, Minderbroedersstraat 10, B-3000 Leuven, Belgium, and Centre for Bioinformatics, School of Life Sciences, Pondicherry University, Puducherry 605014, India

Received August 24, 2009; E-mail: Arnout.Ceulemans@chem.kuleuven.be

Abstract: Synthetic biology and systems chemistry demonstrate a growing interest in modified nucleotides to achieve an enzymatically stable artificial nucleic acid. A potential candidate system is xylose-DNA, in which the 2′-deoxy-β-D-ribo-furanose is substituted by 2′-deoxy-β-D-xylo-furanose. We present here the helical structure and conformational analysis of xylose-DNA on the basis of 35 ns MD simulations of a 29-base-pair DNA duplex. Starting from a right-handed xylose-DNA helix, we observe a remarkable conformational transition from right- to left-handed helix. The left-handed xylose-DNA is highly dynamic, involving screwing and unscrewing motion of the helix. The sugar pucker induced helical changes influence the backbone to adopt the backbone angles for xylose-DNA while retaining the Watson−Crick base pairing and stacking interactions. The results demonstrate the chiral orthogonality of the ribose and xylose based episomes. As far as stability and compactness of information storage is concerned, the ribose based natural DNA is unsurpassed.

1. Introduction

The marvelous helical structure of DNA continues to attract broad interest. Modification of the nucleic acid backbone influences the geometry of the double helix. Such modifications have been introduced to increase the enzymatic stability and the hybridization properties of the artificial nucleic acids, so that they are better apt to function as antisense or antigene probes.[1] The selection of the modified oligonucleotides that are used for such studies is largely driven by their potential ability to hybridize with natural nucleic acids (single- or double-stranded DNA and RNA). As a result such studies have only envisaged modifications that preserve a right-handed duplex structure. The synthetic efforts have also been concerned with the intriguing question of the origin of the contemporary information system. Here, the focus has been on the synthesis of oligonucleotides composed of monomers in the D-sugar configuration. More recent potential applications of modified nucleic acids can be found in the emergent research directions of synthetic biology and systems chemistry. Synthetic biology asks for the development of new tools to safely modify organisms, and this could be based on the development of new (in vivo) information systems, orthogonal to (in the aspect that it lacks communication with) the natural DNA/RNA system. The study of self-replication (systems chemistry), however, needs the development of synthetic nucleic acids that may occur in different duplex conformations (of different stability) when hybridized with itself.

From the chemical point of view, the development of artificial analogues of natural DNA involves major modifications at either the Watson−Crick base pairing or sugar-phosphodiester backbone.[2] Recent developments in non-natural bases have been reported by Kool and co-workers.[3] Reports on the modified sugar-phospodiester backbone include, among others, peptide nucleic acids,[4] 2′5′-linked nucleic acids,[5] xylo-derived nucleic acids,[6] locked nucleic acids,[7] threo-furanosyl nucleic acids,[8] hexitol nucleic acids,[9] and phosphorothiolates.[10] The 4′-C substituted oligonucleotides show an increased resistance toward enzymatic degradation, especially the amino-substituted ones. Alternatively, the sugar-modified analogues like p-RNA,[11] homo-DNA,[12] which do not interact with natural nucleic acids, have mainly been studied in the context of the origin of life.

Here we have studied by molecular modeling the dynamics of xylose-DNA, a D-oligonucleotide that occurs in the left handed configuration. Research on xylose-DNA was started by Seela and co-workers,[13−22] who synthesized the xylo-derivative of nucleic acid bases by substituting the 2′-deoxy-β-D-ribo-furanose with 2′-deoxy-β-D-*xylo*-furanose (i.e., changing the

[†] INPAC Institute and Quantum Chemistry Laboratory.
[‡] Laboratory for Medicinal Chemistry.
[§] Pondicherry University.

(1) Proske, D.; Blank, M.; Buhmann, R.; Resch, A. *Appl. Microbiol. Biotechnol.* **2005**, *69*, 367–374.
(2) Micklefield, J. *Curr. Med. Chem.* **2001**, *8*, 1157–1179.
(3) Krueger, A. T.; Lu, H.; Lee, A. H. F.; Kool, E. T. *Acc. Chem. Res.* **2007**, *40*, 141–150, and previous publications.
(4) Nielsen, P. E. *Chem. Biodivers.* **2007**, *4*, 1996–2002.
(5) Horowitz, E. D.; Hud, N. V. *J. Am. Chem. Soc.* **2006**, *128*, 15380–15381.
(6) Ravindra Babu, B.; Raunak; Poopeiko, N. E.; Juhl, M.; Bond, A. D.; Parmar, V. S.; Wengel, J. *Eur. J. Org. Chem.* **2005**, *11*, 2297–2321.
(7) Wengel, J.; Petersen, M.; Frieden, M.; Koch, T. *Lett. Pept. Sci.* **2004**, *10*, 237–253.
(8) Heuberger, B. D.; Switzer, C. *Org. Lett.* **2006**, *8*, 5809–5811.
(9) Lescrinier, E.; Esnouf, R.; Schraml, J.; Busson, R.; Heus, H. A.; Hilbers, C. W.; Herdewijn, P. *Chem. Biol.* **2000**, *7*, 719–731.
(10) (a) Eckstein, F. *Annu. Rev. Biochem.* **1985**, *54*, 367–402. (b) Egli, M.; Pallan, P. S. *Annu. Rev. Biophys. Biomol. Struct.* **2007**, *36*, 281–305.
(11) Pitsch, S.; Wendeborn, S.; Jaun, B.; Eschenmoser, A. *Helv. Chim. Acta* **1993**, *76*, 2161–2183.
(12) Egli, M.; Lubini, P.; Pallan, P. S. *Chem. Soc. Rev.* **2007**, *36*, 31–45.

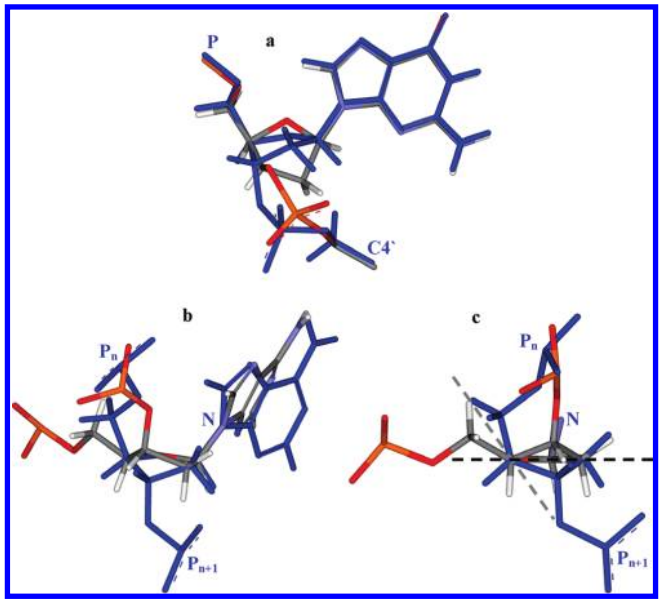

Figure 1. Superimposition of xylo-nucleotide and ribo-nucleotide (blue). Part (a) represents the superimposition of initial xylo-nucleotide template over the ribo-nucleotide (colored blue). Part (b) represents the superimposition of final xylo-nucleotide over the ribo-nucleotide (colored blue) and a side view from C3′-atom (c) is shown, without the base, to clearly depict the change in xylose-DNA backbone. The black axis that passes through the plane of sugar and the gray axis reflect the change in backbone dihedral angles of xylose-DNA in comparison with natural B-DNA.

sugar puckering from C2′-*endo* to C3′-*endo*) and studied their structural and biological characteristics (Figure 1). Optical asymmetry of DNA is due to the C1′, C3′, and C4′ carbons and in xylose, the C3′ is inverted with respect to ribose. The resulting xylose-DNA is thus a diastereoisomer of the natural DNA. Incorporation of a single 2′-deoxy-β-D-xyloguanosine (xG) in the nucleotide string d(G-G-C-A-xG-A-A-G-A-C) significantly decreased the duplex stability, and the introduction of few xylo-configured nucleotides as d(xC-xC-G-T-xC-T-T-xC-T-G) negatively influenced the hybridization properties.[13−22] However, the fully modified self-complementary 2′-deoxy -*xylo*-configured oligo-nucleotides, d(xG-xT-xA-xG-xA-xA-xT-xT-xC-xT-xA-xC-T) expressed similar stability to that of natural DNA.[22] The work on sequence dependent duplex flexibility as a function of backbone configuration highlighted the importance of modified backbone structure in designing antisense oligonucleotides.[23] Most importantly, a spectroscopic analysis of oligo(2′-deoxy-β-D-*xylo*-nucleotide), d(xG-xT-xA-xG-xA-xA-xT-xT-xC-xT-xA-xC-T) revealed a mirror-image-like Circular Dichroism (CD) compared to the regular counterpart[22] suggesting the formation of a left-handed double helix as a consequence of C3′-endo puckering.

The helix transition from right- to left-handed duplex and the relevant modifications in backbone configuration would greatly affect the biological properties of xylose-DNA and therefore influence its applications in antisense and antigene therapeutics.[23] To date the X-ray crystallographic data and structural information on such therapeutically important xylose-DNA are not yet available. In the present contribution, we study the conformational aspects of xylose-DNA with the aid of molecular dynamics (MD) simulation.

MD simulation is currently complementing experimental structure techniques and takes advantage beyond the experimental limit when a complete description on the dynamics of a (bio)molecule is needed. In particular, MD of DNA in explicit water and ions has been successfully applied to a range of problems with accurate treatment of the long-range electrostatic interactions.[24−27] Despite the existing limitations like ion convergence and lack of polarizability due to semiempirical force fields, the all-atom MD simulations are performing well to analyze the biomolecular properties beyond the experimental limit.[28] MD produces stable trajectories of fully solvated DNA over multinanosecond time scales with structures close to crystallographic and NMR data.[29] It has been successfully applied to understand the conformational transition from B- to A-form[30] and also to Z-form of DNA.[31] The conformational transition induced by the salt concentration is well- documented using MD analysis.[32] MD has proven its ability even to identify the sequence dependent conformational perturbation in DNA.[33]

Using MD, we simulate here the geometrical changes induced by the incorporation of the xylo-furanose moiety in the B-form of DNA (B-DNA). Hereafter, we call this xylo-furanose substituted B-DNA as xylose-DNA. The xylose-DNA is designed by replacing all the 2′-deoxy-β-D-ribo-furanose with 2′-deoxy-β-D-xylo-furanose and dissolved in a water medium with sufficient counterions to mimic the biological environment. All-atom MD simulations for a period of 35 ns have been performed using AMBER8.0 with parm99 force field parameter database[34] for canonical B-DNA and RESP partial charges derived at 6-31G* level for xylose-DNA, to identify the type of new conformation adopted and its stability.

(13) Rosemeyer, H.; Seela, F. *Helv. Chim. Acta* **1991**, *74*, 748–760.
(14) Seela, F.; Rosemeyer, H.; Krecmerovà, M.; Roling, A. *Nucleic Acids Res. Symposium Series* **1991**, *24*, 87–90.
(15) Rosemeyer, H.; Krecmerova, M.; Seela, F. *Helv. Chim. Acta* **1991**, *74*, 2054–2067.
(16) Krecmerova, M.; Seela, F. *Nucleosides Nucleotides* **1992**, *11*, 1393–1409.
(17) Rosemeyer, H.; Strodtholz, I.; Seela, F. *Bioorg. Med. Chem. Lett.* **1992**, *2*, 1201–1206.
(18) Seela, F.; Wörner, K.; Rosemeyer, H. *Collect. Czech. Chem. Commun.* **1993**, *58*, 150.
(19) Seela, F.; Wörner, K.; Rosemeyer, H. *Helv. Chim. Acta* **1994**, *77*, 883–896.
(20) Rosemeyer, H.; Seela, F. *Nucleosides Nucleotides* **1995**, *14*, 1041–1045.
(21) Schöppe, A.; Hinz, H. J.; Rosemeyer, H.; Seela, F. *Eur. J. Biochem.* **1996**, *239*, 33–41.
(22) Seela, F.; Heckel, M.; Rosemeyer, H. *Helv. Chim. Acta* **1996**, *79*, 1451–1461.
(23) Crooke, S. T., Ed. In *Handbook of Experimental Pharmacology: Antisense Research and Applications*: Springer: New York, 1995.
(24) Cheatham, T. E., 3rd; Miller, J. J.; Fox, T.; Darden, T. A.; Kollman, P. A. *J. Am. Chem. Soc.* **1995**, *117*, 4193–4194.
(25) Beveridge, D. L.; McConnell, K. J. *Curr. Opin. Struct. Biol.* **2000**, *10*, 182–196.
(26) Cheatham, T. E., 3rd; Kollman, P. A. *Annu. Rev. Phys. Chem.* **2000**, *51*, 435–471.
(27) Cheatham, T. E., 3rd; Young, M. A. *Biopolymers* **2001**, *56*, 232–256.
(28) Cheatham, T. E., 3rd *Curr. Opin. Struct. Biol.* **2004**, *14*, 360–367.
(29) Norberg, J.; Nilsson, L. *Q. Rev. Biophys.* **2003**, *36*, 257–306.
(30) Pastor, N. *Biophys. J.* **2005**, *88*, 3262–3275.
(31) Kastenholz, M. A.; Schwartz, T. U.; Hünenberger, P. H. *Biophys. J.* **2006**, *91*, 2976–2990.
(32) Song, C.; Xia, Y.; Zhao, M.; Liu, X.; Li, F.; Ji, Y.; Huang, B.; Yin, Y. *J. Mol. Model* **2006**, *12*, 249–254.
(33) Guliaev, A. B.; Sagi, J.; Singer, B. *Carcinogenesis* **2000**, *21*, 1727–1736.
(34) Cheatham, T. E., 3rd; Cieplak, P.; Kollman, P. A. *J. Biomol. Struct. Dyn.* **1999**, *16*, 845–862.

2. Materials and Methods

In this section, we provide detailed information on the modeling of xylose-DNA and the selection of the DNA sequence. We describe the protocol for the MD simulations and the methods for structural analysis.

2.1. Modeling Xylose-DNA. The sugar puckering in B-DNA is C2′-endo (S-type conformation) and is C3′-endo (N-type conformation) in A-DNA,[35] whereas the xylo-configured nucleotides adopt N-type conformation[13,15] similar to A-DNA.

The xylo-modification in DNA sugar moiety has been introduced by (i) changing the sugar puckering from C2′-endo to C2′-exo and C3′-exo to C3′-endo (i.e., the C2′-endo sugar puckering of B-DNA has been changed to C3′-endo of A-form and hence this modification was not required in A-DNA), (ii) the positions of O3′- and H3′-atoms connected to C3′ were interchanged so that the atoms O3′ and O5′ lie on the same side of the pentose ring, and (iii) the positions of the backbone atoms from O3′ to C5′(i.e., O3′, P, O1P, O2P, O5′, C5′, H5′1, and H5′2) are adjusted so that the DNA continues to have the similar phosphodiester linkage with O3′-atom as in natural DNA. A template of xylo-configured nucleotide with the above-mentioned modifications has been designed separately for B- as well as for A-DNA and was used to build the complete xylo-derivative of DNA using Xleap of AMBER 8.0. For the intermediate DNA conformation between A- and B-form, only the O3′-atom was flipped up to stay in the N-type conformation and the backbone atoms were perfect to accommodate such configuration without any distortions in the backbone atoms from O3′ to C5′. The superimposition of initial xylo-nucleotide template (colored by atoms) over the ribo-nucleotide (blue) is shown as Figure 1a in the article.

2.2. Xylose-DNA Conformations Studied. As a preliminary step, analysis on xylose-DNA is invoked by replacing all the 2′-deoxy-β-D-ribo-furanose of a 13-base-pair natural DNA duplex, d(G-T-A-G-A-A-T-T-C-T-A-C-T)[22] with the xylo-configured counterpart, i.e., 2′-deoxy-β-D-xylo-furanose, and the resulting model of xylose-DNA is d(xG-xT-xA-xG-xA-xA-xT-xT-xC-xT-xA-xC-T). Using this sequence, both the A-form and B-form of xylose-DNA have been modeled and used for the MD simulation. The conformational evolution of this xylose-DNA has been studied using MD simulations both in explicit and implicit solvation.

Having analyzed the stability of these duplexes, this study has further been extended with the experimentally crystallized 29-base-pair B-DNA of sequence; 5′-d(G-T-A-T-A-T-T-C-C-C-T-C-G-G-G-A-T-T-T-T-T-T-A-T-T-T-T-G-T)-3′ and the resulting xylose-DNA is denoted as 5′-d(xG-xT-xA-xT-xA-xT-xT-xC-xC-xC-xT-xC-xG-xG-xG-xA-xT-xT-xT-xT-xT-xT-xA-xT-xT-xT-xT-xG-T)-3′.[36]

2.3. Protocol of MD Simulations in Explicit Solvation. All atom MD simulations for a period of 35 ns have been performed using AMBER8.0 with parm99 force field parameter database[34] for canonical B-DNA. For xylose-DNA, RESP partial charges[37] derived at 6-31G* level using Gaussian03[38] have been used for the simulations. (Supporting Information, Table S1).

The newly modeled xylose-DNA conformation was minimized for a few cycles in order to remove the initial strains. After relaxation, the xylose-DNA was solvated using TIP3P water molecules[39] in a box of size 66.461 × 54.554 × 54.498 Å for the 13-mer, and 45.963 × 122.373 × 50.124 Å for the 29-mer. The molecular extent for the initial right-handed as well as the simulated left-handed duplex of 13-mer and 29-mer varies as 40 ± 2 and 99 ± 1 Å, respectively. Negative charges were neutralized by Na^+ ions to mimic the real system. The particle-mesh Ewald procedure is used to handle long-range electrostatic interactions.

To start with, the system was gradually relaxed from artificial strains by performing minimization first only for the solvent water molecules, then releasing the constraints on the end base-pairs simultaneously from both ends and finally minimizing the complete system using a cutoff distance of 8 Å. The system was heated to 300 K for 50 ps with harmonic restraints of 2 kcal/mol/ Å^2 on xylose-DNA at constant volume and then maintained at 300 K using the Langevin dynamics[40−42] with a collision frequency of 1.0 ps^{-1}. The hydrogen bonds were constrained using the SHAKE algorithm.[43] The density of the system was equilibrated for 200 ps at constant pressure in steps of 50 ps simulation and the harmonic constraint on xylose-DNA was removed by reducing 0.5 kcal/mol/Å^2 of harmonic constraint in every 50 ps simulation and finally equilibrated for 50 ps without any constraints. After equilibration, the entire system was allowed for MD production runs under constant pressure conditions for 35 ns.

2.4. Protocol of Generalized Born Simulations. Additionally solvent effects in Generalized Born (GB) simulation (implicit solvation) were modeled implicitly using the modified GB model of Onufriev et al.[44] implemented in Amber 8. The dielectric constants of 1 and 78.5 were used for the interior DNA and the outer solvent regions, respectively. The nonpolar solvation free energy was calculated using the solvent accessible surface area model[45] with a surface tension of 0.005 kcal mol^{-1} Å^{-2}. Salt effects were accounted at a salt concentration of 0.2 M using an extension of the GB model to include Debye−Hückel theory.[46] Temperature was regulated through use of Langevin dynamics[40−42] with a collision frequency of 1.0 ps^{-1}. The cutoff distance of 15 Å is used for the nonbonded interactions.

A short minimization on DNA was performed using 500 steps of conjugate gradient method, while the constraints on the base pairs were gradually released in every 50 steps starting from the terminal base pairs, and followed by a similar minimization on completely relaxed DNA. The system was then heated to 300 K using a 2.0 fs time step for 50 ps with harmonic restraints on all DNA atoms using a weight constant 2.0 kcal mol^{-1} Å^{-2}. The density of the system was equilibrated gradually for 200 ps at constant pressure and in every 50 ps of simulation the harmonic constraint on xylose-DNA was reduced by 0.5 kcal/mol/Å^2 and finally equilibrated without any constraints for another 50 ps and followed by the production runs of simulation.

2.5. Structural Analysis. The conformational energies were extracted from the SANDER output files. The MD trajectory files have been used to extract: (i) the root-mean-square deviations (rmsd) from the starting conformations, and (ii) the conformations averaged over the last 100 ps of each 1 ns simulation. These averaged conformations have been used for the analysis of: (i) hydrogen bonding in base pairs, (ii) solvent accessible surface area (SASA), and (iii) geometrical parameters like sugar puckering, backbone and glycosyl conformations, groove widths, intrastrand phosphate−phosphate distances, helical parameters, and helix bending. The SASA has been calculated

(35) Saenger, W. *Principles of Nucleic Acid Structure*; Springer: New York, 1984.
(36) Braddock, D. T.; Louis, J. M.; Baber, J. L.; Levens, D.; Clore, G. M. *Nature* **2002**, *415*, 1051–1056.
(37) Bayly, C. I.; Cieplak, P.; Cornell, W. D.; Kollman, P. A. *J. Phys. Chem.* **1993**, *97*, 10269–10280.
(38) Frisch, M. J. et al. *Gaussian 03, Revision D.02*, Gaussian, Inc., Wallingford CT, 2004.
(39) Jorgensen, W. L.; Chandrasekhar, J.; Madura, J. D.; Impey, R. M.; Klein, M. L. *J. Chem. Phys.* **1983**, *79*, 926–935.
(40) Pastor, R. W.; Brooks, B. R.; Szabo, A. *Mol. Phys.* **1988**, *65*, 1409–1419.
(41) Loncharich, R. J.; Brooks, B. R.; Pastor, R. W. *Biopolymers* **1992**, *32*, 523–535.
(42) Izaguirre, J. A.; Catarello, D. P.; Wozniak, J. M.; Skeel, R. D. *J. Chem. Phys.* **2001**, *114*, 2090–2098.
(43) Ryckaert, J. P.; Ciccotti, G.; Berendsen, H. J. C. *J. Comput. Phys.* **1977**, *23*, 327–341.
(44) Onufriev, A.; Bashford, D.; Case, D. A. *Proteins* **2004**, *55*, 383–394.
(45) Weiser, J.; Shenkin, P. S.; Still, W. C. *J. Comput. Chem.* **1999**, *20*, 217–230.
(46) Srinivasan, J.; Trevathan, M. W.; Beroza, P.; Case, D. A. *Theor. Chem. Acc.* **1999**, *101*, 426–434.

using the dms program of Richards[47] in MidasPlus package.[48] The geometrical parameters such as helical parameters, backbone and glycosyl conformations have been calculated using the CURVES program[49] and for sugar puckering and intrastrand $P_i - P_{i+1}$ and $C_i - C_{i+1}$ distances, the 3DNA program[50] has been used. All of these analyses have been performed by excluding the last three terminal base pairs of xylose-DNA to avoid end effects (the intermittent breaking of hydrogen bonds and opening of the terminal base-pair).[51,52] Molecular graphics images were produced using the UCSF Chimera package from the Resource for Biocomputing, Visualization, and Informatics at the University of California, San Francisco.[53]

2.6. Calculation of Groove Widths. The groove width of xylose-DNA is highly varying throughout the dynamics and the numbers of base pairs forming the major and minor grooves are different from the previously reported nucleic acid conformations. Hence, a distance scan between the two strands has been performed to explain the variation in groove width.

In regular B-DNA, the base pairs are sandwiched between the phosphate atoms of the two complementary strands and hence the phosphate atoms become the reference atoms for groove width analysis. The minor groove is formed between n and $n + 3$ base pairs and the major groove is between n and $n + 6$ base pairs. This procedure to determine the groove width is not directly transferable to xylose-DNA. In the left-handed xylose-DNA, the phosphate atoms are flipped toward the major groove and hence the sugar moiety is exposed at the entrance of the minor groove forming the real minor groove width. Thus, we have selected the C4′-atoms as reference atoms for the minor groove width. However, the major groove remains well-defined by the phosphate atoms similar to other nucleic acids. For the calculation, a simple distance scanning between the i^{th} C4′-atom on strand1 (reference atom) and the 10 up- and downstream C4′-atoms (i.e., $i \pm 10$) in strand 2 has been performed. Several trials were also made by changing the reference C4′-atoms. For a comparative analysis, we have also calculated the groove widths using the P-atoms as reference points. The shortest distance determines either the minor or the major groove widths depending on the grooves over which the distance is measured.

3. Results and Discussion

3.1. Preliminary Study of the Effect of Xylose on Natural DNA. Initially, we studied a fully xylo-configured 13-base-pair duplex of DNA, d(G-T-A-G-A-A-T-T-C-T-A-C-T) in both A- and B-form.[22] A further 12-base-pair duplex, (5′-d(C-A-T-G-G-G-C-C-C-A-T-G)-3′) in an intermediate state between A- and B-form was also studied.[54] Despite the difference in the starting conformation, the helical structure in both cases unscrewed so as to form a very similar open form with flexible end groups (Supporting Information, Figure S1). Upon continuing the simulation in implicit solvent a left-handed helix was spontaneously formed within 3 ns (Supporting Information, Figure S2a). Details on MD simulations performed in implicit and explicit solvent medium are given in the Supporting Information. For a complete description of the helicity of left-handed xylose-DNA, this 12/13-base-pair strand is considered to be too short. For further analysis, we turned to a longer sequence.

3.2. Conformational Evolution of Left-Handed Xylose-DNA from Right-Handed B-DNA. We selected a 29-mer model, based on the experimentally crystallized 29-base-pair B-DNA;[36] 5′-d(G-T-A-T-A-T-T-C-C-C-T-C-G-G-G-A-T-T-T-T-T-T-A-T-T-T-T-G-T)-3′. The fully substituted xylose analogue of this 29-mer was constructed from a right-handed B-DNA template in a water box, and simulated for 35 ns. Here we present the results observed for this 29-base-pair xylose-DNA along with a comparison to the natural 29-base-pair B-DNA.

The observed evolution of the 29-base-pair xylose-DNA starting from a B-DNA configuration is shown as a series of snapshots extracted from the MD simulation (Figure 2). The starting right-handed conformation unwinds and opens to a large extent until 8.5 ns and then the helix starts to adopt left-handedness as the system evolves over the time dynamics. Superimposition of the xylose-incorporated DNA conformations at 8.5 ns (right handed duplex) and 9.5 ns (left-handed duplex) highlights the conformational transition from right- to left-handedness (Figure 2). The introduction of the left-handedness starts at the end base-pairs and quickly propagates to the inner duplex. At a later stage the duplex in the complete left-handed form expresses consistent screwing and unscrewing mechanisms throughout the dynamics and hence discloses the highly dynamic nature of xylose-DNA. Apparently, the inversion of one asymmetrical carbon is sufficient to change the handedness of the helical structure. Movies on conformational evolution of xylose-DNA and additional structural data can be accessed from our Web site http://quantchem.kuleuven.be/amutha/. The aim of the subsequent analysis will be to determine which factors trigger the rotation of the handedness. In the process, we also obtain additional insight into the unrivalled structure of the natural DNA itself.

3.3. Geometry of Xylose-DNA. The primary structural element is the relative rigidity of the base-pairing. Xylose-DNA retains the complementary Watson−Crick (H-bond) base pairing similar to B-DNA (Supporting Information, Figure S3 and Table S2). The sugar puckering angles; ν_0, ν_1, ν_2, ν_3, and ν_4 of xylose-DNA stabilize after 15 ns (Figure 3a) and are closer to the reported values from potential energy calculations[35] (Supporting Information, Table S3). The simulated B-DNA falls in the range of reported values from fiber diffraction[55] data for natural B-DNA. The compound parameter which provides a concise description of the conformational state of the sugar is the pseudo rotation phase (P) and is calculated from the endocyclic sugar torsion angles as

$$\tan P = \frac{(\nu_4 + \nu_1) - (\nu_3 + \nu_0)}{2 \cdot \nu_2 \cdot (\sin 36^\circ + \sin 72^\circ)}$$

Almost concomitant with the helix transition from right to left, we observe a conformational switch from C2′-endo (160 ± 10°) to C3′-endo (10 ± 10°), but with a different time scale for different nucleotides (Figure 3b).

The backbone dihedrals (alpha-α, beta-β, gamma-γ, delta-δ, epsilon-ϵ, zeta-ζ) and glycosyl dihedral (chi-χ) angles of simulated xylose-DNA and B-DNA are compared with the dihedral angles from X-ray diffraction data of B-DNA[56]

(47) Richards, F. M. *Annu. Rev. Biophys. Bioeng.* **1977**, *6*, 151–176.
(48) Ferrin, T. E.; Huang, C. C.; Jarvis, L. E.; Langridge, R. *J. Mol. Graphics* **1988**, *13*−*27*, 36–37.
(49) Lavery, R.; Skelnar, H. *J. Biomol. Struct. Dyn.* **1988**, *6*, 63–91.
(50) Lu, X.-J.; Olson, W. K. *Nucleic Acids Res.* **2003**, *31*, 5108–5121.
(51) Leroy, J. L.; Kochoyan, M.; Huynh-Dinh, T.; Gueron, M. *J. Mol. Biol.* **1988**, *200*, 223–238.
(52) Nonin, S.; Leroy, J. L.; Guéron, M. *Biochemistry* **1995**, *34*, 10652–10659.
(53) Pettersen, E. F.; Goddard, T. D.; Huang, C. C.; Couch, G. S.; Greenblatt, D. M.; Meng, E. C.; Ferrin, T. E. *J. Comput. Chem.* **2004**, *25*, 1605–1612.
(54) Ng, Ho-L.; Kopka, M. L.; Dickerson, R. E. *Proc. Natl. Acad. Sci. U.S.A.* **2000**, *975*, 2035–2039.

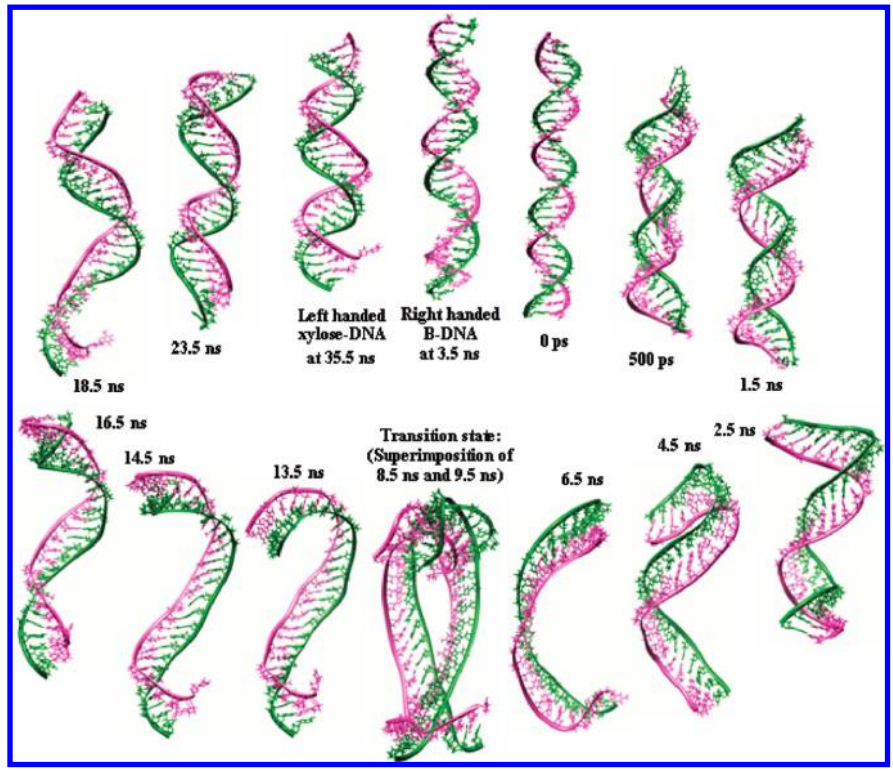

Figure 2. Conformational evolution of left handed xylose-DNA derived from 29-base-pair B-DNA. The evolution of helix transition through out the dynamics is shown with some selective conformations for clarity in the clock-wise direction. The transition state from R- to L-form is depicted by the superposition of conformations at 8.5 ns and 9.5 ns.

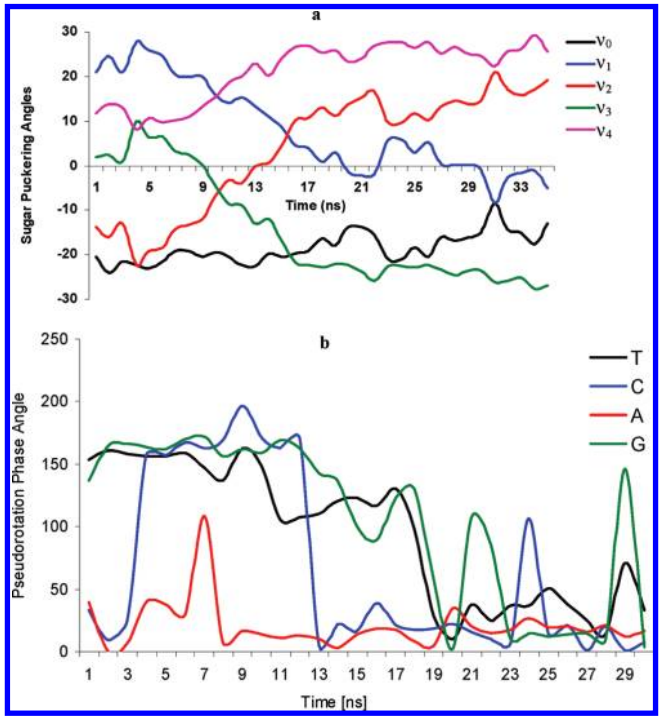

Figure 3. Evolution of C3′-endo from C2′-endo during MD-simulation. Part (a) shows the variation in the five sugar puckering torsion angles; ν_0, ν_1, ν_2, ν_3, and ν_4 and (b) depicts the variation in Pseudorotation phase (P) angles of the four nucleic bases in xylose-DNA during MD simulation.

(Supporting Information, Figure S4 and Table S4). The dihedral angle α fluctuates as +50 ± 15° and ζ expresses a consistent value of +80 ± 10° throughout the dynamics. Prior to the modification in backbone dihedral angle, the angle χ stabilizes first to −86 ± 4° at 5 ns (−98.0° in B-DNA) indicating the rearrangements in the orientation of the base pairs relative to the sugar moiety as the first phenomenon. The sequential order in adopting the characteristic β, γ, δ, and ϵ angles of xylose-DNA are as follows: γ to −135 ± 15° at 14 ns (−165° in ZI-DNA), δ to −30 ± 2° after 16 ns, ϵ to 120° after 17 ns (177.7° in A-DNA), β to −130 ± 20° after 17 ns; α and ζ are in +syn clinal (−syn clinal in B-DNA), β is in −anti clinal (+anti clinal in B-DNA) and ϵ is in +anti clinal (−anti clinal in B-DNA). The torsion angle γ is in −anti periplanar (+syn periplanar in B-DNA) and δ is in −syn clinal (+anti clinal in B-DNA). The χ is in −syn clinal (−anti clinal in B-DNA). The dihedral angles α and β of xylose-DNA are in good agreement with the left-handed double helices reported by Albiser and Premilat.[57] The dihedrals γ and δ adopt a new conformation as a consequence of helix transition induced by the change in sugar puckering from R- to L-form. The dihedral angles of the simulated B-DNA are in good agreement with the reported angles except the dihedral angle ζ.

The helical parameters describing the local and global translational and rotational displacements of the base steps as well as base pairs have been listed in Supporting Information, Tables S5and S6. Among the global base pair axis parameters, the inclination of xylose-DNA is high (i.e., +24 ± 6°, which is 0.0 ± 2.0° in B-DNA), while the X-, Y-displacements and tip fall in the range of natural DNA (Supporting Information, Table S5). The base−base step parameters: shear, stretch, stagger, buckle, propeller-twist, and base openings show distinctive

(55) Sasisekaran, V.; Gupta, G.; Bansal, M. *Int. J. Biol. Macromol.* **1981**, *3*, 2–8.
(56) Arnott, S.; Chandrasekaran, R.; Birdsall, D. L.; Leslie, A. G. W.; Ratcliff, R. L. *Nature* **1980**, *283*, 743–745.
(57) Albiser, G.; Premilat, S. *Nucleic Acids Res.* **1982**, *10*, 4027–4034.

behavior in xylose-DNA (Supporting Information, Figure S5 and Table S5); when xylose-DNA is compared to the canonical B-DNA, the propeller twist and stagger have been identified as the influencing parameters triggering the helical change since their direction is reversed at equal amplitude. There is also a swing in the direction of stretch which fluctuates closer to zero. The shear, buckle, and base opening fluctuate closer to the values of B-DNA.

The geometry of xylose-DNA measured from the interbase-pair parameters such as slide, rise, roll, and twist are 2.4 Å, 3.45 Å, 5°, and −25°, respectively, and the respective angles in B-DNA are −1.0 Å, 3.4 Å, 2°, and 32° (Supporting Information, Figure S6 and Table S6). The change in the direction of slide and twist discloses their role as one of the major driving sources during the helix transition. The local/global interbase and interbase-pair parameters such as slide, rise, roll, and twist values reveal similar variations during the dynamics on both local and global scale. The local shift and tilt are more illustrative than the global parameters (Supporting Information, Table S6).

In xylose-DNA, the intrastrand P_n.. .P_{n+1} distance is less by 0.85 Å, and the C_n. .. C_{n+1} distance is 0.4 Å higher than B-DNA (Supporting Information, Figure S7). Despite larger conformational fluctuation due to the transition from right- to left-handed helicity, the interstrand C1′-C1′distance between the two strands (10.6 Å) is consistent with the natural B-DNA and reinforces stable base paring in xylose-DNA also. The virtual angle between the C1′−YN1 or C1′−RN9 glycosidic bonds (Y for pyrimidine and R for purine) and the line between C1′−C1′ atoms of both strands measures the elevation of the base pairs with respect to the backbone sugar moiety. The elevation in xylose-DNA is marginally larger by 1° than in natural B-DNA (55.5°).

In xylose-DNA, the minor groove is formed between n and $n + 2$ base pairs with a consistent groove width of 11 Å (Figure 4a) and the major groove is formed between n and $n + 7.5$ base pairs, but the width varies as 45 ± 4 Å (Figure 4b) referring to larger helix flexibility during the dynamics. This is also ensured by the ratio of groove width to the P−P distance (6 Å) in xylose-DNA. Such large conformational changes are reflected by sligthly higher fluctuation in end-to-end distance of xylose-DNA (70 ± 3 Å), when compared to B-DNA is 72 ± 2 Å (Supporting Information, Figure S8).

3.4. Solvent-Accessible Surface Area (SASA). The solvent accessible surface area (SASA) is an essential parameter to understand the hydration role of xylose-DNA. During the simulation of B-DNA, a polar surface of area 3425 Å^2 and a nonpolar surface of area 3300 Å^2 have been observed. The polar and nonpolar atoms of xylose-DNA are equally exposed in their configuration. The polar and nonpolar SASA after 16 ns amounts to 3300 ± 50 Å^2 which matches the nonpolar surface area of B-DNA (Supporting Information, Figure S9). Unlike the B-DNA, where the aromatic bases are buried between the two sugar phosphate backbone strands, the bases in xylose-DNA are highly exposed (1475 ± 25 Å^2) in the major groove and hence are freely accessible for the water molecules, which supports the observation of entropically favorable exposure of nucleobases for solvation by Seela et al.[19] It is interesting to observe that the polar SASA of backbone, major and minor groove in xylose-DNA are almost the same (725 ± 25 Å^2) and the sugar contributes the least for solvation (100 ± 25 Å^2). Similarly, the nonpolar SASA of the base is dominating and fluctuates at 2250 ± 25 Å^2 after the helix transition. The nonpolar SASA of the backbone remained unchanged (1350 Å^2) throughout the dynamics. The SASA of sugar and major groove (1450 ± 50 Å^2) fluctuates closer to the SASA of the backbone atoms. The minor groove of xylose-DNA possesses the least SASA (950 Å^2).

3.5. Correlation between the Geometrical Parameters. Clearly in order to understand the mechanism of the helix inversion, we have to examine the correlation between the geometrical parameters. This will reveal the communicative dynamics between the structural elements: base-pair stacks, sugar linkages, and backbone (Figure 5). As far as the base pairs are concerned, the inclination is more pronounced than in B-DNA. Among the base-step parameters, the pronounced positive propeller twist influences the clockwise rotation of the upper base for the helical transition along with stagger movements. And, when both propeller twist and stagger move toward the positive direction, the stretch swifts to negative direction. The base−base shear, buckle and base opening fluctuate in the same direction as for B-DNA but with equal or little higher amplitude. One of the important parameters involved in the helical change is the twist and its change from positive (for R-form) to negative twist (for L-form) is associated with an increase in the global slide from negative to positive values (Figure 5a), but decreases the local slide (Figure 5b). The local slide and global rise vary linearly (Figure 5c) and as the global slide increases, the local roll decreases (Figure 5d). Similar to slide, the negative shift also changes to positive during the helix transition.

It is indicative that there is a correlation between the sugar puckering phase angle (P) and torsion angle χ over the global inter base-pair slide (Figure 5e). The change in direction of the global slide from negative to positive values is associated with the helix transition and the initial correlation (negative region in Figure 5e) indicates that the helix transition is derived by the coupled action of global base-pair slide and χ and, after the transition the base pairs show a positive slide with a consistent χ angle. Similarly, the sugar puckering phase angle also equally correlates with slide and reaches to a value of 50° (for C3′-endo). It is also important to add that xylose-DNA possesses a positive slide similar to the BII conformation,[58] which is one of the conformational substrates of B-DNA playing a key role in DNA−protein recognition.

The torsion angle χ defining the orientation of sugar with respect to the glycosyl C1′-N link and the backbone torsion angle ϵ, defining the rotation of C4′-C3′-O3′-P, are highly correlated and consistent throughout the dynamics (Figure 5f). The circled points correspond to the conformations of left-handed xylose-DNA (having the high anti-χ between −80 and −86° and ϵ between 112 and 126°). The correlation between χ and ϵ reveals the simultaneous communication during the time evolution between characteristic xylo-rotation and the base pair orientation with respect to the sugar moiety.

The variation of local interbase rise, tilt and roll that are associated with the vertical separation of the bases influences the van der Waals (VDW) interaction between the stacked bases of DNA[59] (Supporting Information, Figure S6) and their stable variation after the helix transition reveals the existence of the stable base stacking interactions. In the helix of xylose-DNA, the effective rotation of C3′-endo sugar puckering reduces the

(58) Hartmann, B.; Piazzola, D.; Lavery, R. *Nucleic Acids Res.* **1993**, *21*, 561–568.
(59) Hunter, C. A.; Lu, X.-J. *J. Mol. Biol.* **1997**, *265*, 603–619.

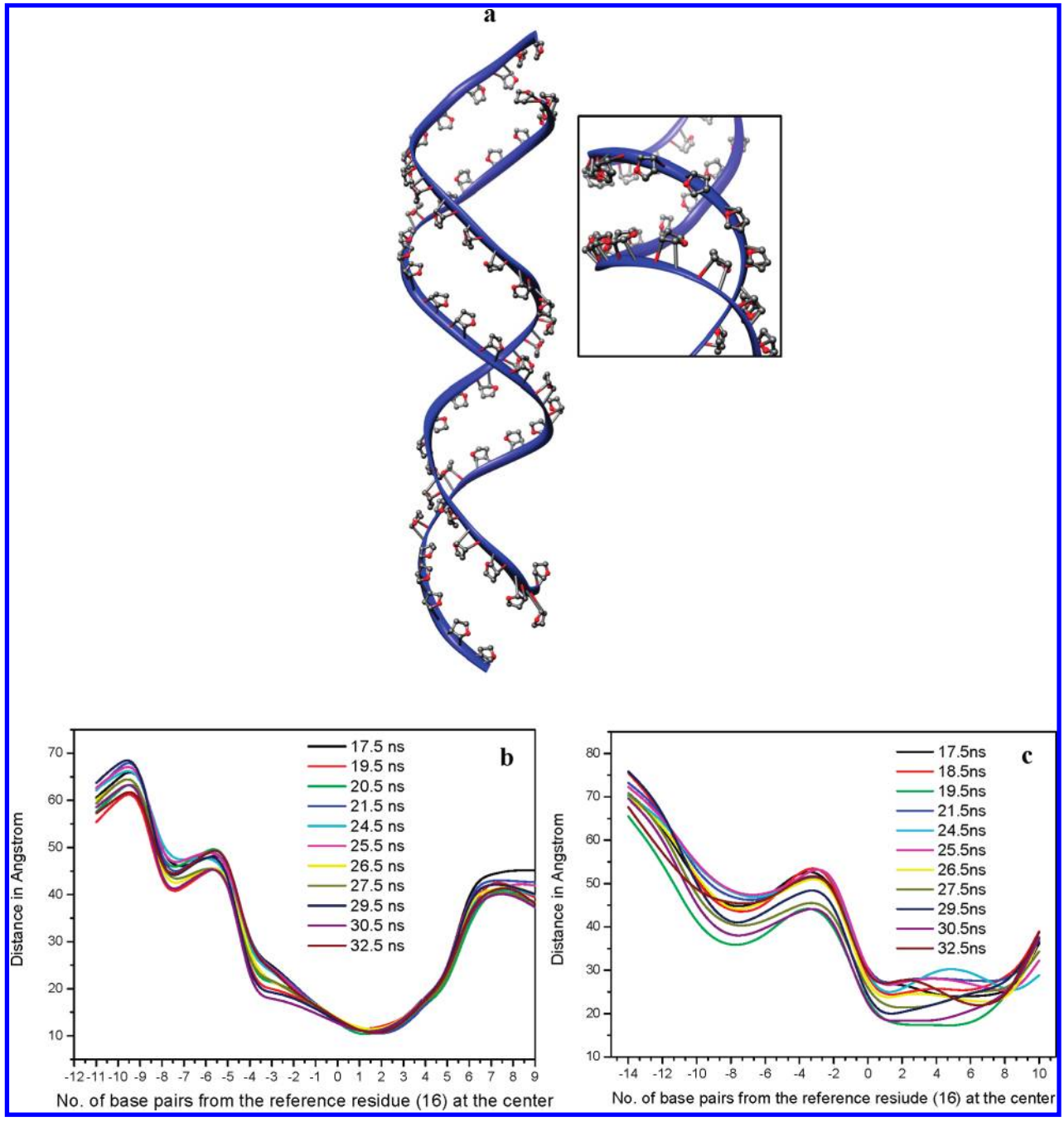

Figure 4. Groove width of xylose-DNA. The base-pairs in xylose-DNA are concealed to explain the participation of sugar moiety in the minor groove and the presence of Phosphate in the major groove like natural DNA (a) and the subset depicts a closer view of minor groove. The groove width calculated using C4′-atom of xylo-furanose (b) and the backbone P-atom (c) is plotted.

(P_n.. .P_{n+1}) distances, increases the (C_n.. .C_{n+1}) distances, and increases the elevation of base pairs with respect to the sugar moiety by 1° while maintaining similar C1′−C1′ distance between the strands. The polar and nonpolar SASA are equally exposed and hence the polar SASA of xylose-DNA duplex could accommodate ∼12 water molecules less than B-DNA assuming 10 Å^2 for each water molecule.[60]

(60) Parsegian, V. A.; Rand, R. P.; Rau, D. C. *Methods Enzymol.* **1995**, *259*, 43–94.

4. Conclusions

The replacement of the sugar moiety, 2′-deoxy-β-D-ribo-furanose of a nucleotide in B-DNA with a 2′-deoxy-β-D-xylo-furanose has revealed the conformational transition of right-handed B-DNA to a left-handed duplex, xylose-DNA. During the simulation of 35 ns, the 2′-deoxy-β-D-xylo-furanose incorporated initial duplex takes about 18 ns for a complete transition from right- to left-handed duplex and subsequently remains as a left-handed duplex throughout the simulation. After the conformational transition, the xylose-DNA duplex constantly expresses a screwing and unscrewing motion in

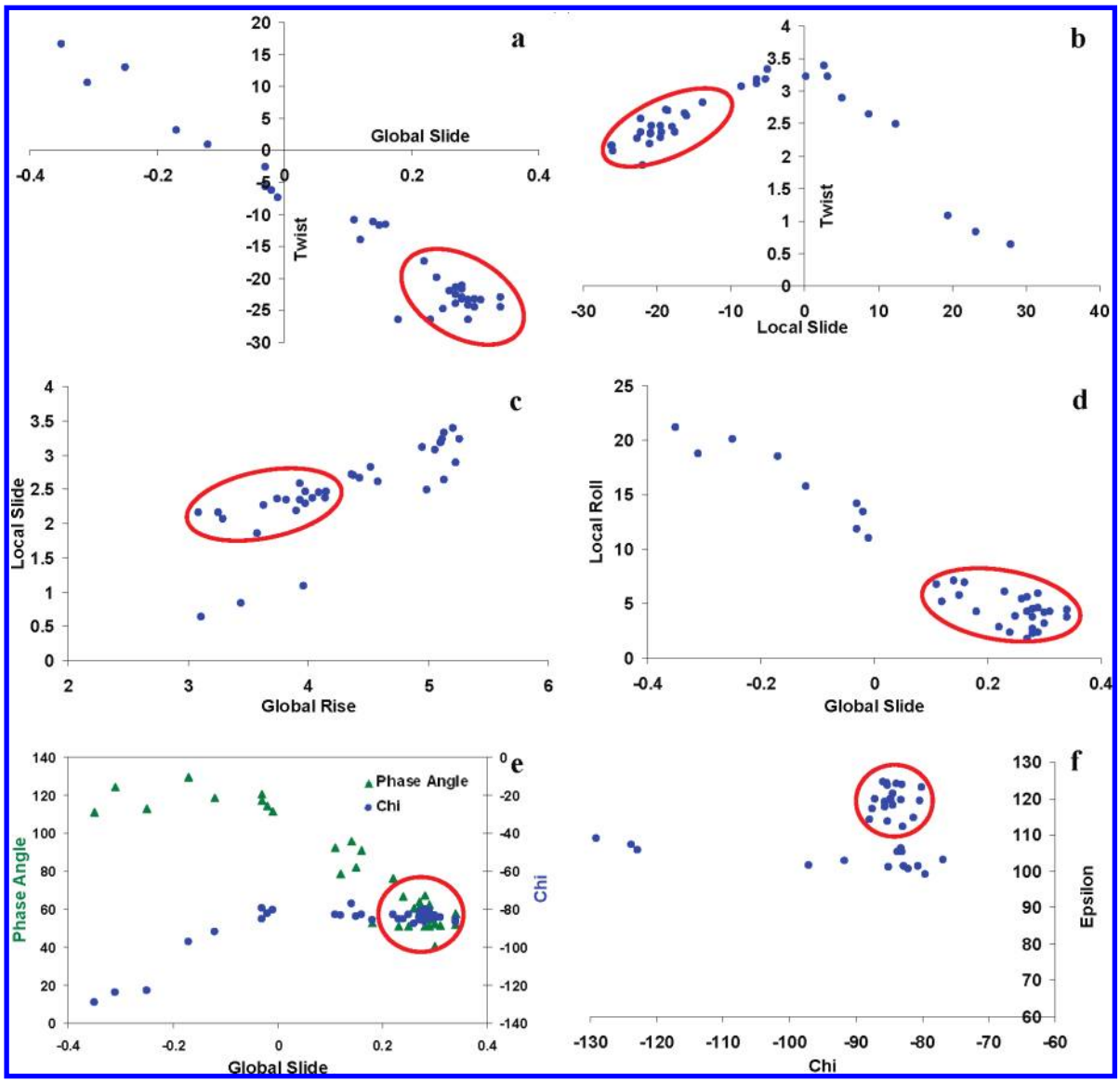

Figure 5. Communicative helical parameters during the course of MD simulations. The correlation between; twist Vs global slide (a), twist Vs local slide (b), local slide Vs global rise (c), global slide Vs local roll (d), global slide Vs phase angle, chi (e), and chi vs epsilon (f) are shown separately. The stabilized left handed xylose-DNA conformations are encircled.

the duplex, which do not alter the H-bonding interaction between the strands and the minor groove width, but do alter the end-to-end distance as well as the major groove width. The transition in sugar puckering from C2′-endo to C3′-endo is mediated by cooperative dynamics between the torsion angles during the simulation and the observed correlated linear variation between the torsion angles (ν_2 and ν_1) and (ν_3 and ν_4) are the examples. The helical backbone angles; α, β, ϵ and ζ reflect the mirror image of the respective angles of B-DNA, except the middle angles; γ and δ, which can be achieved by a clock-wise rotation of 180° in B-DNA. The conclusion which results from this analysis, is that the inversion of one of the carbons in the sugar linkage promotes switching in the handedness of the double helix without amending the strong base-pairing and stacking interactions between the complementary base pairs. This result explains the observation of a mirror image CD spectrum for oligo xylose-DNA.[22] A similar inversion of the CD spectrum is observed during the B-Z transition of natural DNA.[61] Simulation of this transition in explicit solvent required the use of targeted MD.[62]

The relevance of this work may be seen in function of (a) questions about the origin of life and (b) the construction of self-replicating systems. Ribose-DNA forms much more compact and, conformationally, much more stable helical structures than xylose-DNA, which might be an advantage for storage and propagation of information. The conformational instability of the xylose-DNA double helix is a handicap when it comes to biological applications. In the future we will study the conformational dynamics of xylose nucleic acids (xylose-RNA with a 2′ OH) in order to study its potential as "natural" precursor of xylose-DNA. An important question with respect to the origin of the information systems is if xylose-DNA and xylose-RNA show similar conformational flexibility and similar conformational preferences.

One of the problems with autocatalytic self-replication systems is product inhibition, leading to parabolic instead

of exponential amplification.[63] Sequence (or length) dependent conformational mobility based on backbone alterations, might avoid product inhibition. To validate this hypothesis, it will be important to investigate the use of xylose-DNA as template for self-replication, based on a ligase reaction.[64] An important study, therefore, is the systematic investigation of the sequence specificity of the conformational flexibility of xylose-DNA (finding its precedent in the B to Z transitions in natural DNA, and features such as A-tract bending).

From the point of view of synthetic biology, it would be interesting to study to which extent the triphosphates of xylose nucleosides are accepted as a substrate for polymerases. These studies are in progress.

Acknowledgment. Financial support from the Flemish Government through the Concerted Action Scheme is gratefully acknowledged. We also thank Dr. S. Moors and Mr. S. Michielssens for valuable suggestions.

Supporting Information Available: An Appendix with five Tables (S1−S6) and nine Figures (S1−S9) is given to support the observations reported herein. This material is available free of charge via the Internet at http://pubs.acs.org.

JA9065877

(61) Kypr, J.; Kejnovská, I.; Renèiuk, D.; Vorlièková, M. *Nucleic Acids Res.* **2009**, *37*, 1713–1725.
(62) Kastenholz, M. A.; Schwartz, T. U.; Hünenberger, P. H. *Biophys. J.* **2006**, *91*, 2976–2990.
(63) Luther, A.; Brandsch, R.; von Kiedrowski, G. *Nature* **1998**, *396*, 245–248.
(64) Sievers, D.; von Kiedrowski, G. *Chem.—Eur. J.* **1998**, *4*, 629–641.